Supplementary Information for

Wireless microwave-to-optical conversion via programmable metasurface without DC supply

Xin Ge Zhang[1#], Ya Lun Sun[1#], Bingcheng Zhu[2#], Han Wei Tian[1], Bo Yuan Wang[1], Zaichen Zhang[2,3,4]*, Cheng-Wei Qiu[5]*, Tie Jun Cui[1,6]*, and Wei Xiang Jiang[1,3,4]*

[1] State Key Laboratory of Millimeter Waves, School of Information Science and Engineering, Southeast University, Nanjing 210096, China
[2] National Mobile Communications Research Laboratory, School of Information Science and Engineering, Southeast University, Nanjing 210096, China
[3] Frontiers Science Center for Mobile Information Communication and Security, Southeast University, Nanjing 210096, China
[4] Purple Mountain Laboratories, Nanjing 211111, China
[5] Department of Electrical and Computer Engineering, National University of Singapore, Singapore, 117583, Singapore
[6] Suzhou Laboratory, Suzhou 215000, China

These authors contributed equally: Xin Ge Zhang, Ya Lun Sun, Bingcheng Zhu.

E-mail: zczhang@seu.edu.cn, chengwei.qiu@nus.edu.sg, tjcui@seu.edu.cn, wxjiang81@seu.edu.cn

This Supplementary Information file includes:

Supplementary Figures 1 to 13

Supplementary Notes 1 to 9

Supplementary Figures

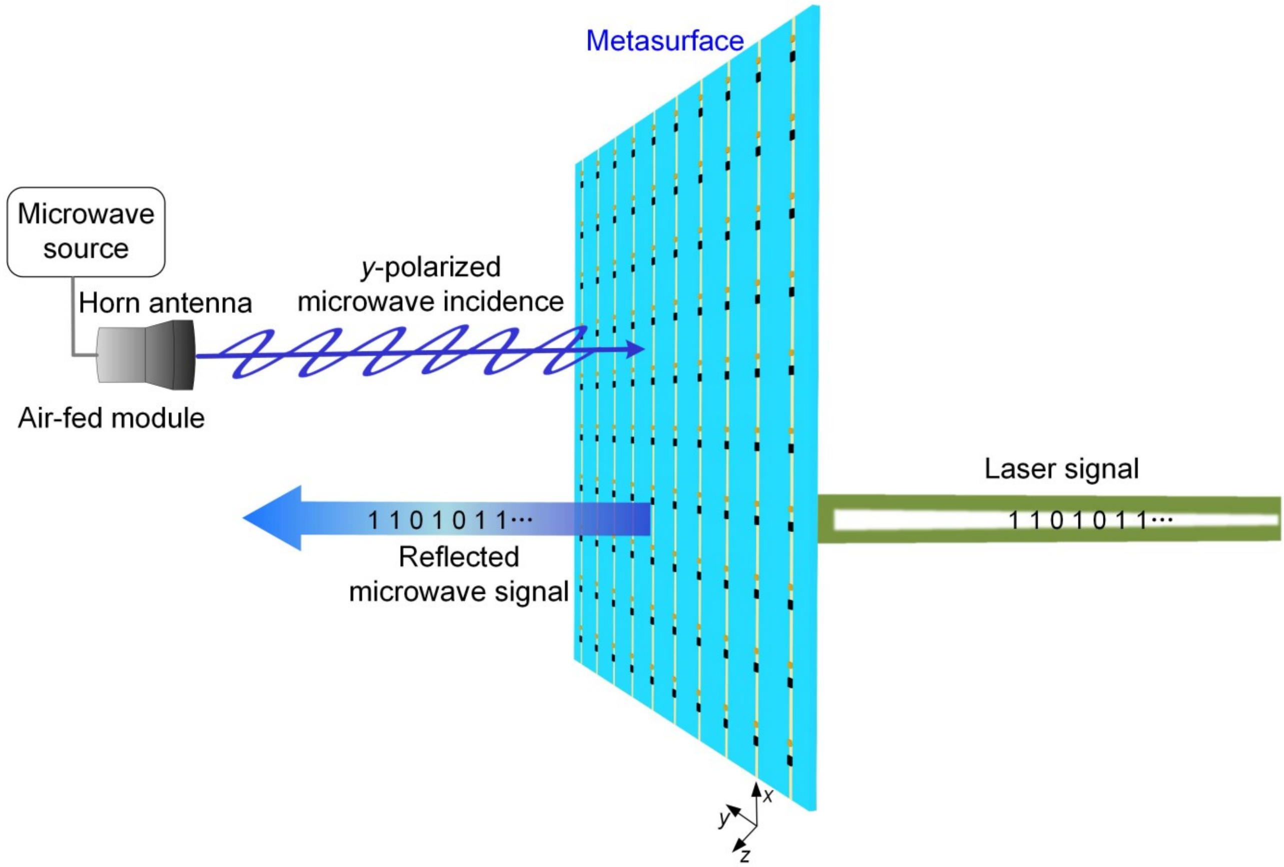

Supplementary Figure 1. Schematic of the metasurface-based optical-to-microwave conversion. An air-fed module consisting of a microwave source and a connected high-directional horn antenna is adopted to provide required incident microwave.

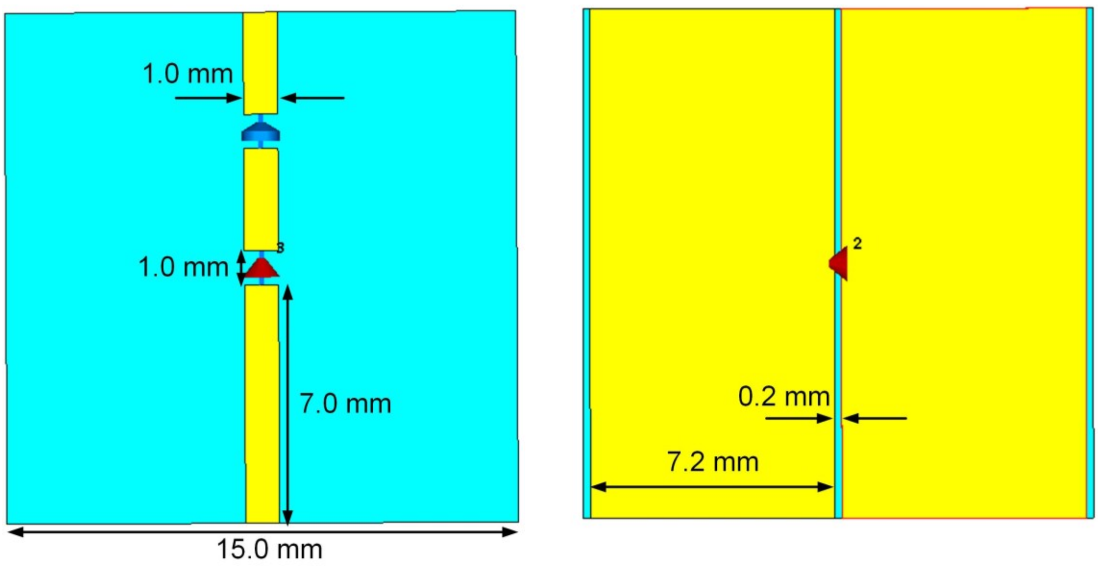

Supplementary Figure 2. Simulation model of meta-element with the optimized structure parameters. The structure parameters were optimized to reach high absorptivity and large reflection amplitude difference.

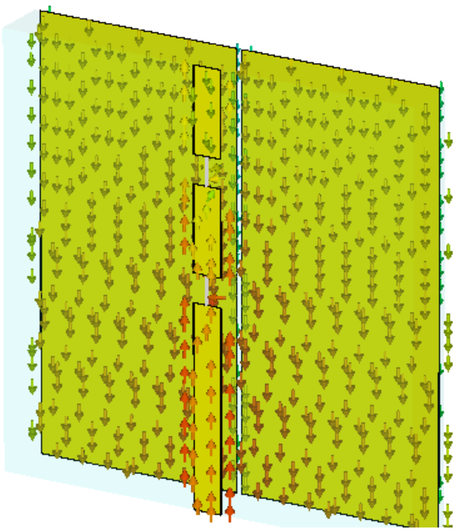

Supplementary Figure 3. Simulated induced surface-current distribution of the meta-element at 4.06 GHz. It is clear that the strong surface-current is induced on the Resonant Structure 1 under x-polarized microwave incidence, which will generate a potential across the loaded Schottky diode to drive it on.

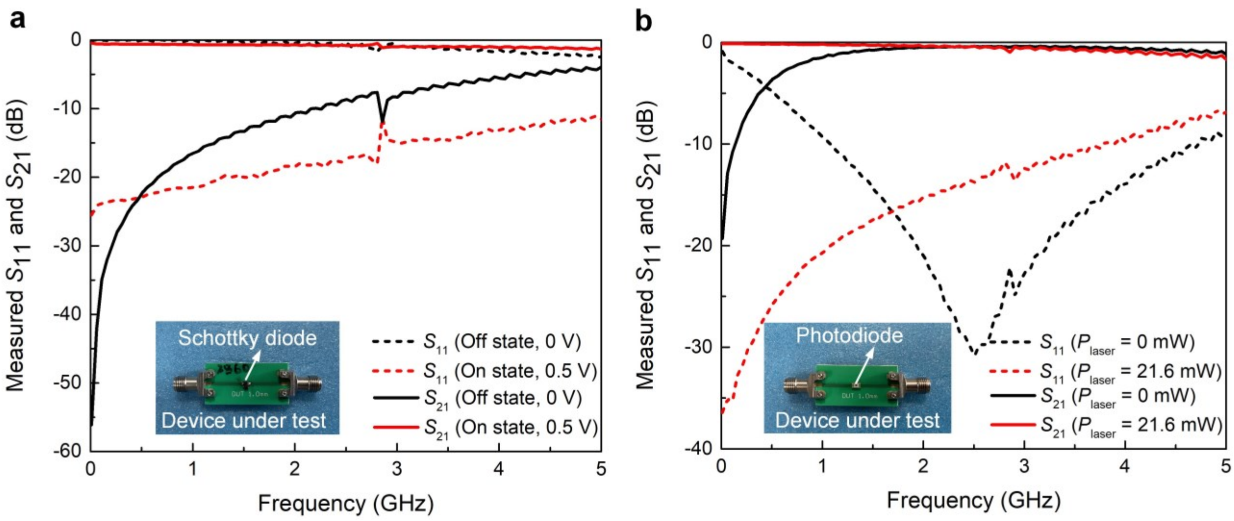

Supplementary Figure 4. Measured *S*-parameters of two diodes based on TRL calibration method. a, Measured S_{11} and S_{21} curves of the Schottky diode (HSMS-2860) under the off and on states. **b**, Measured S_{11} and S_{21} curves of the photodiode (S13773) under the illumination of green lasers with two different powers of 0 and 21.6 mW.

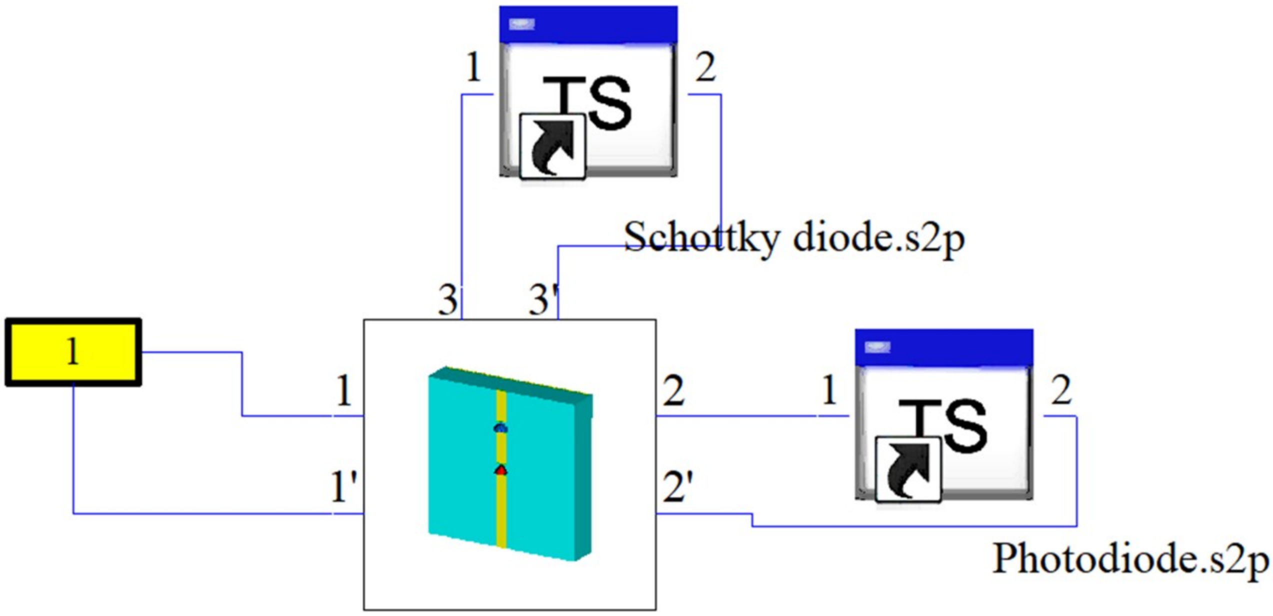

Supplementary Figure 5. Field-circuit co-simulation model of the meta-element. The photodiode and Schottky diode are modeled as discrete Ports 2 and 3, respectively, in which the measured *S*-parameters can be imported directly through the TS modules.

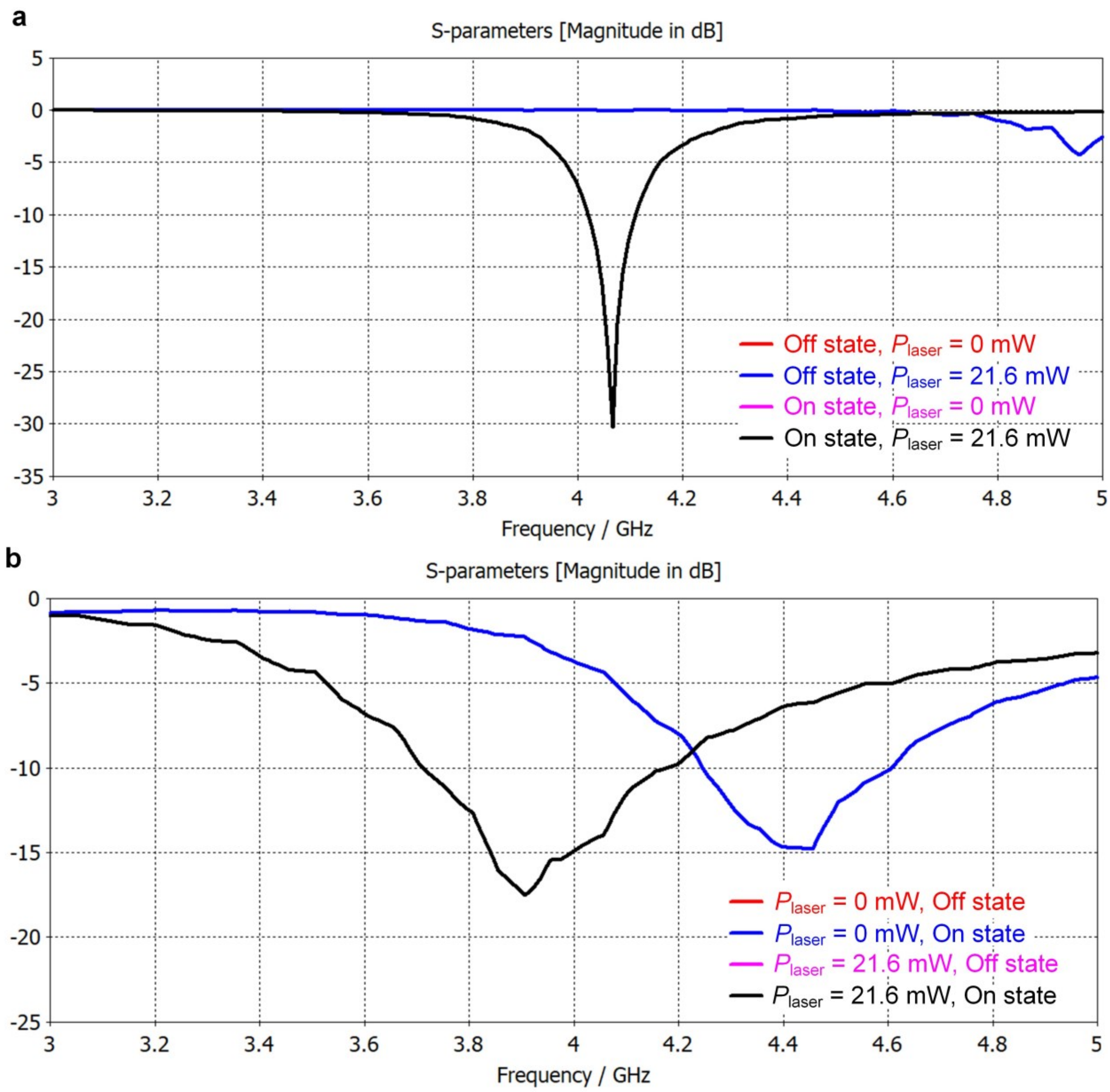

Supplementary Figure 6. Simulated reflection amplitudes of the meta-element with different configurations under *x*- and *y*-polarized microwave incidences to evaluate cross polarization isolation. a, For *x*-polarized microwave incidence, changing the state of the photodiode in the cross-polarization direction has no effect on the resonance response. **b**, For *y*-polarized microwave incidence, changing the state of the Schottky diode in the cross-polarization direction has no effect on the resonance response.

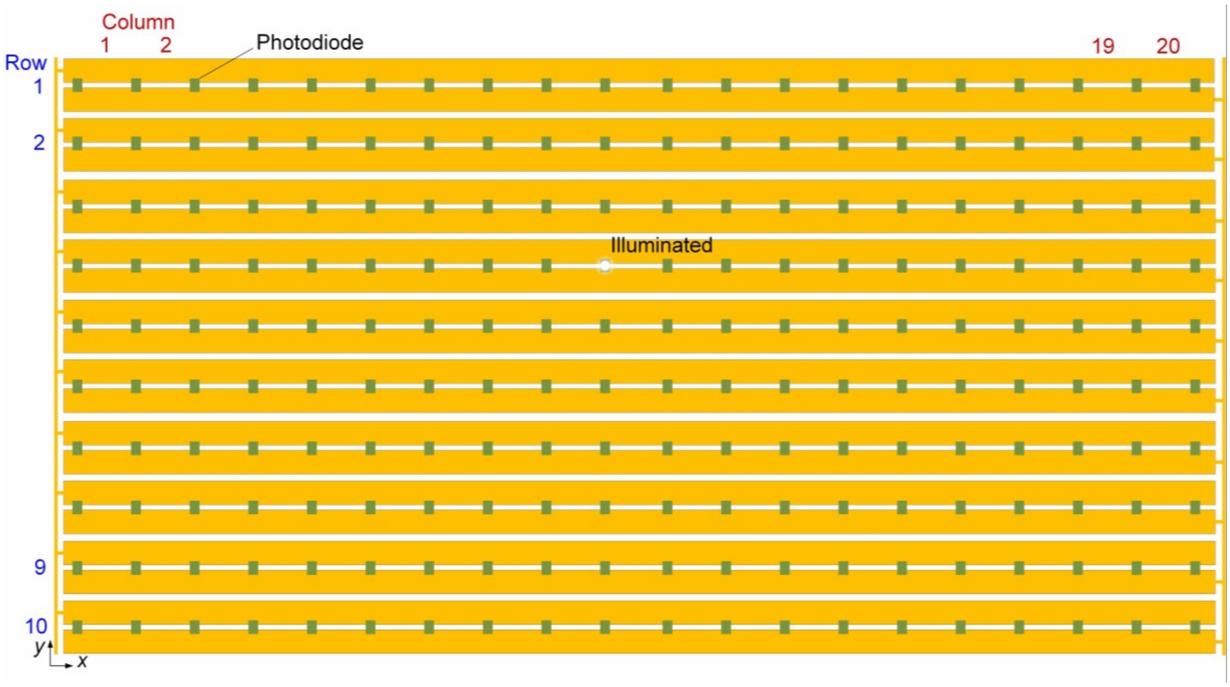

Supplementary Figure 7. Schematic of the photodiode-based optical-to-microwave conversion structures and their connection relationship. All the photodiodes are connected in parallel, and thus any one of them can be illuminated to drive the metasurface to work.

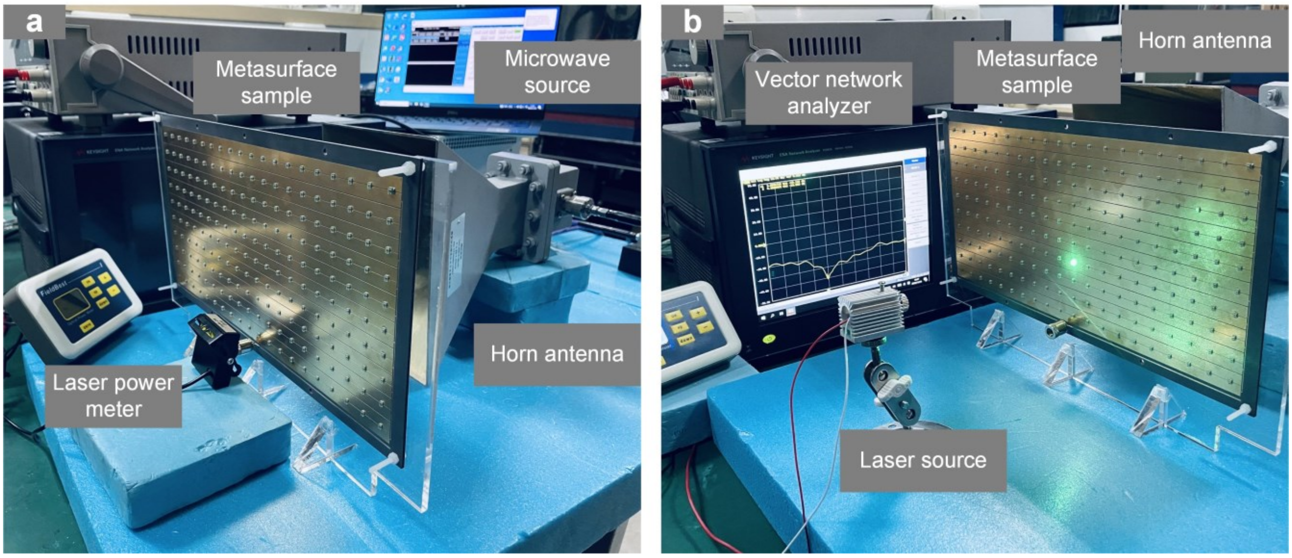

Supplementary Figure 8. Experimental setups on microwave-laser bidirectional conversion. a, Experimental setup for the microwave-to-laser up-conversion. **b**, Experimental setup for the laser-to-microwave down-conversion.

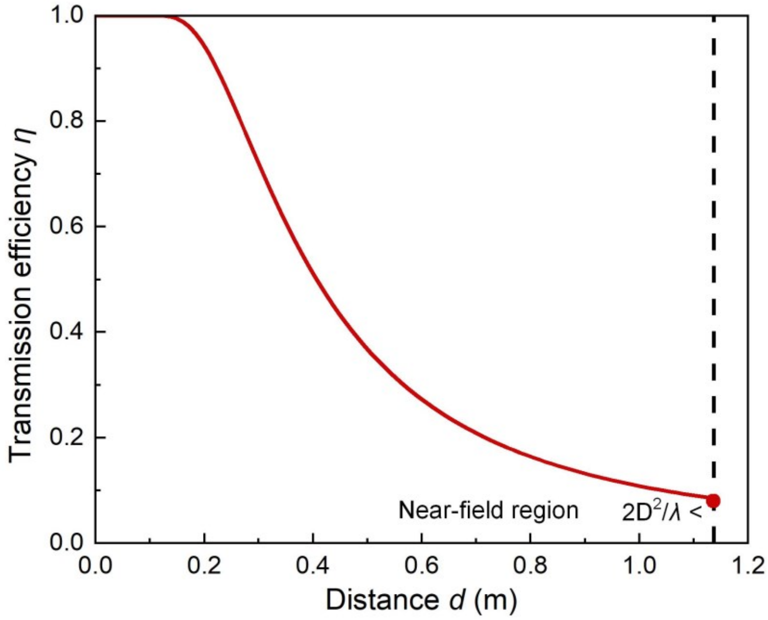

Supplementary Figure 9. Calculated microwave transmission efficiency *η* at near field with different antenna distances *d*. When the antenna distance *d* is small, the transmission efficiency can reach nearly 100%.

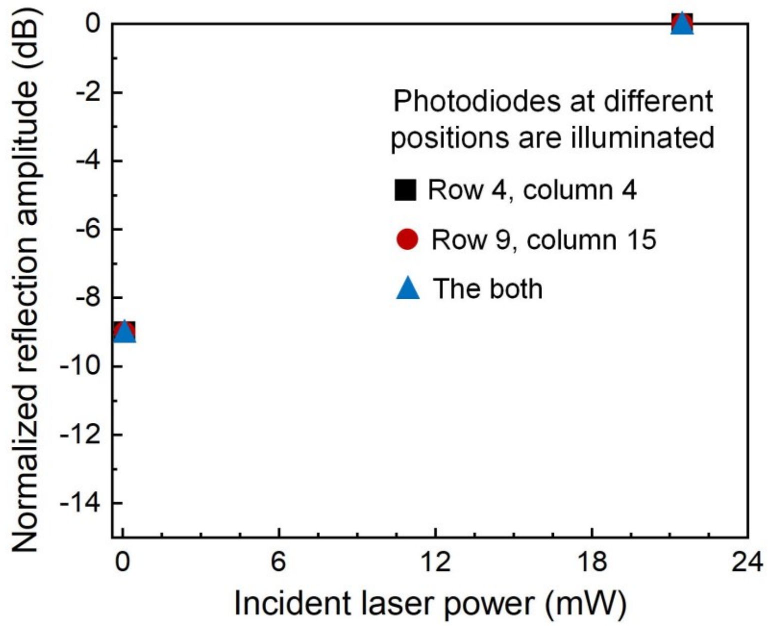

Supplementary Figure 10. Normalized measured microwave reflection amplitudes of the metasurface at 4.45 GHz when photodiodes at different positions are illuminated. It is clear that the metasurface can generate the same microwave reflection amplitude differences when photodiodes at other positions are illuminated.

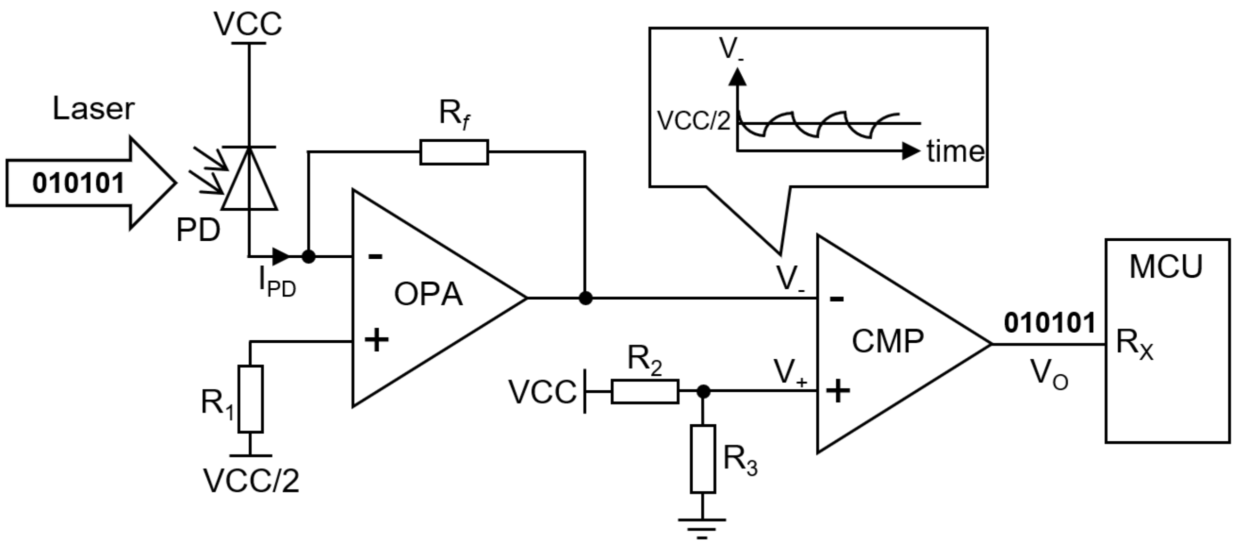

Supplementary Figure 11. Simplified diagram of the designed photoelectric detection and demodulation circuit. The laser detection and demodulation functions are integrated into one circuit.

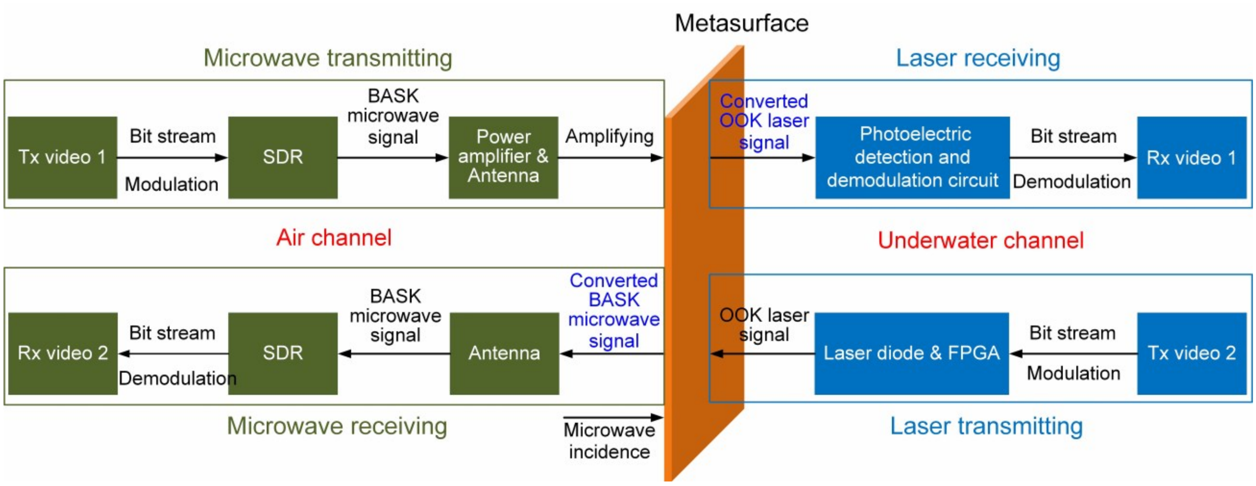

Supplementary Figure 12. Workflow of the full-duplex air-water wireless communication system with the hybrid microwave and laser links. Video 1 can be transmitted from air and then well be received underwater through the microwave-to-laser wireless link; Video 2 can be transmitted from the underwater and then be well received in air through the laser-to-microwave wireless link. Importantly, these two video transmissions are conducted simultaneously and independently.

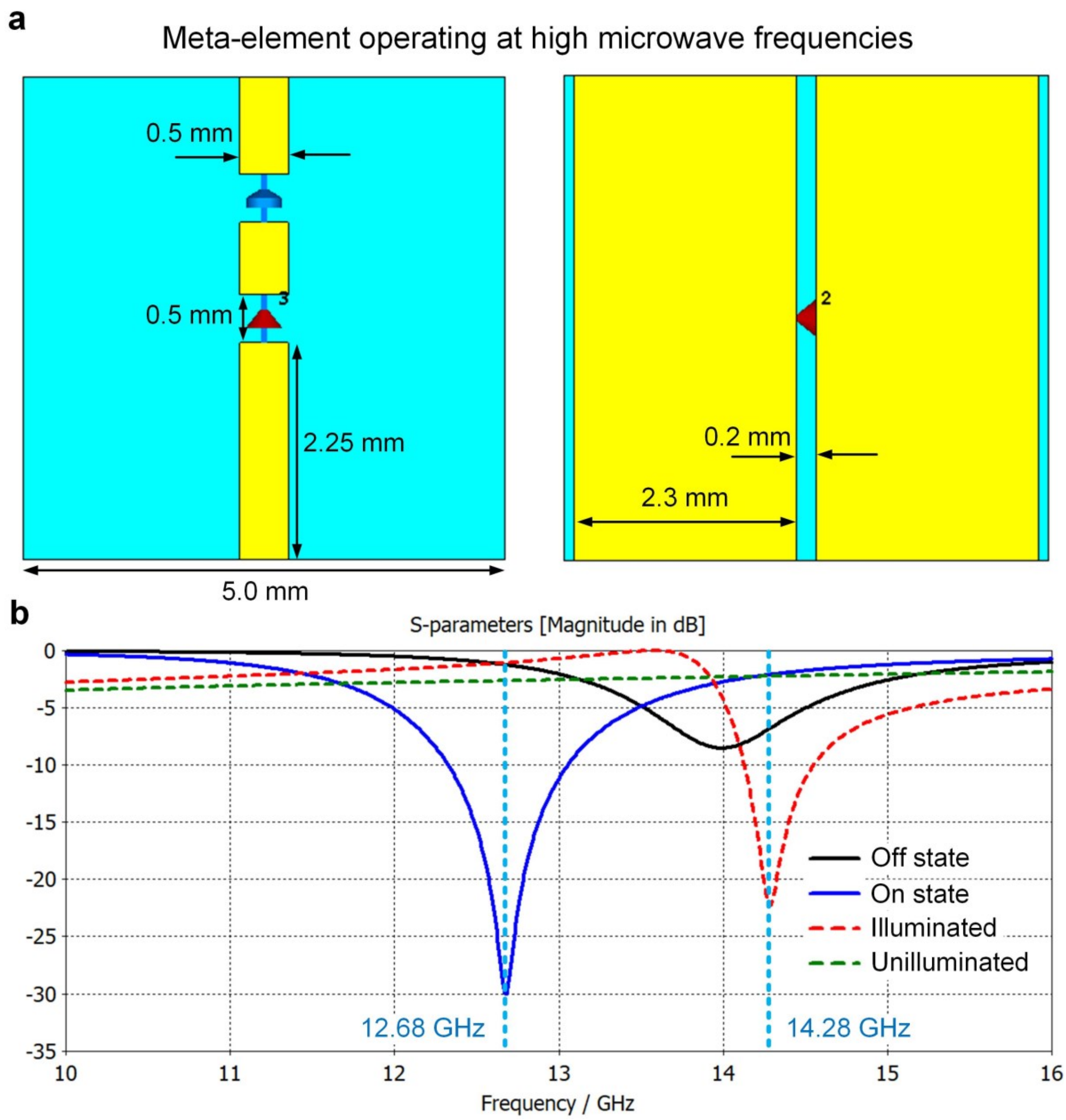

Supplementary Figure 13. Optimized meta-element based on high cut-off frequency Schottky diode and photodiode for achieving higher microwave frequencies. a, Simulation model of the high-frequency meta-element with a side length of 5.0 mm and a substrate thickness of 1.0 mm. **b**, Simulated microwave reflection amplitudes of the meta-element under different working states of Schottky diode and photodiode.

Supplementary Notes

Supplementary Note 1. Microwave incidence method

The optical-to-microwave conversion is achieved by using laser to modulate the reflection characteristics of incident microwave. In our demonstration, we adopt directly the air-fed module that contains a microwave source and a connected high-directional horn antenna to provide required incident microwave, as shown in Supplementary Fig. 1. The source emits the microwave signal, which is then transmitted through the horn antenna to illuminate the metasurface. The active air-fed scheme is very effective and is often used in the metasurface implementation because it can provide stable microwave incidence, including required polarization, frequency and power. Besides the common air-fed approach, some metasurfaces have also been investigated recently to receive passively EM waves from environment, such as Wi-Fi signals[1] and remote base-station signals[2]. These attempts provide more possibilities for feeding methods of metasurfaces, and are helpful to reduce the power consumption of the overall system.

For the air-fed module, the received microwave power P_r by the metasurface can be calculated by the Friis transmission equation[3]:

$$P_r = \frac{G_t A_m}{4\pi d^2} P_t \tag{S1}$$

where P_t is transmitted power, G_t is the gain of the horn antenna, A_m is the effective aperture of the metasurface, and d is the distance between the horn antenna and the metasurface. Therefore, the transmission efficiency η can be calculated by:

$$\eta = \frac{P_r}{P_t} = \frac{G_t A_m}{4\pi d^2} \tag{S2}$$

in addition, to generate quasi-plane wave incidence, the distance d needs to satisfy far-field condition:

$$d > \frac{2D^2}{\lambda} \tag{S3}$$

where D is the aperture of the antenna, and λ is the wavelength in free space. According to Eq. (S2), for the fabricated metasurface and the selected horn antenna, the transmission efficiency η depends on the distance d. As the distance increases, the transmission efficiency decreases.

Supplementary Note 2. Diode selection and testing

To achieve efficient metasurface-enabled microwave-laser interactions, the used diodes must be able to work well in the microwave band and have high sensitivity. We here choose the photodiode (S13773) to implement the meta-element due to low junction capacitance and wide spectral response. In our previous work[4], we have demonstrated that the photodiode can interact well with microwave metasurface, and it can be used as a tunable capacitor under different light intensities. We chose to use the Schottky diode (HSMS-2860) due to low threshold voltage and large power capacity.

In general, an equivalent resistor-inductor-capacitor (RLC) circuit can be used to mimic the diode, however, it is easy to ignore the influence of parasitic parameters, such as package inductance. Unlike this approximate simulation method, we test directly the scattering parameters (S-parameters) of the diode to characterize it. To achieve the accurate S-parameters of the Schottky diode and photodiode under different states, we adopt the through-reflect-line (TRL) calibration method. The fabricated device under test (DUT) of the Schottky diode and its measured S_{11} and S_{21} curves under two different states are shown in Supplementary Fig. 4a. From transmission coefficients S_{21}, we see clearly that the Schottky diode exhibits different transmission characteristics under the on and off states. We note that in the diode test, we directly use external voltages to change the diode states, but in the metasurface operation, the on/off states of the Schottky diode are switched by the incident microwave powers, without any external power supply connection. We also fabricated the DUT of the photodiode and its measured S_{11} and S_{21} curves for two different laser powers are shown in Supplementary Fig. 4b. It is obvious that the microwave transmissions have been changed under different illuminations, resulting in a red shift due to an increase in the junction capacitance.

Supplementary Note 3. Meta-element simulation

To use the measured *S*-parameters to perform meta-element simulation, we here adopt field-circuit co-simulation method, and the established simulation model is shown in Supplementary Fig. 5. In the simulations, the Schottky diode and the photodiode are modeled as two discrete ports, in which the measured *S*-parameters can be imported directly. That is to say, the Schottky diode and the photodiode are represented by their measured *S*-parameters. Therefore, we can obtain the microwave resonance responses of the meta-element under different cases by changing the input *S*-parameters.

Supplementary Note 4. Near-field transmission efficiency

There is a strong relationship between the required microwave power and the antenna distance d, as free-space loss has a significant impact on microwave transmission efficiency. To improve transmission efficiency and reduce the input microwave power, for microwave-to-laser conversion, we consider placing the horn antenna in the near-field region. In this case, the microwave transmission efficiency can be calculated using the following formula[5]:

$$\eta = \frac{P_r}{P_t} = 1 - \mathrm{e}^{-\tau^2} \tag{S4}$$

where $\tau^2 = G_t A_m / 4\pi d^2$, which is closely related to distance d. P_t and P_r are the transmitted microwave power from the antenna and the received microwave power of the metasurface, respectively. In the microwave-to-optical conversion experiment, the gain G_t of used horn antenna is 15 dBi and effective metasurface area A_m is 300 × 150 mm^2. In this case, the calculated transmission efficiencies η at near field with different distances d are plotted in Supplementary Fig. 9. It is clear that in the near-field region, when the antenna distance d is small, the transmission efficiency can reach nearly 100%.

In video transmission experiments, we first placed the horn antenna 0.1 m away from the metasurface sample (Case 1), and the corresponding transmission efficiency η is 99.9%. Then, as a demonstration, we increased the antenna distance to about 0.3 m (Case 2), and at the same time, we increased the transmission power by 2.0 dB. For both cases, the hybrid communication system can work well, as presented in Supplementary Movie 1.

Supplementary Note 5. Working principle of photoelectric detection and demodulation circuit

The schematic diagram of the designed photoelectric detection and demodulation circuit is shown in Supplementary Fig. 11. When the photodiode receives the modulated OOK laser signal, it generates a nA-level photocurrent $\mathrm{I_{PD}}$, which is too small to be directly detected. Therefore, the photocurrent is amplified by a following operational amplifier (OPA), and the generated current signal $\mathrm{I_{PD}}$ is converted to a voltage signal V_{-}. The amplifier gain is characterized by $V_{-} = \frac{\mathrm{VCC}}{2} - \mathrm{R}_f * \mathrm{I_{PD}}$ and the light-induced voltage $-\mathrm{R}_f * \mathrm{I_{PD}}$ is on the level of tens of mV, which is ready to be detected by the following comparator (CMP). This CMP compares the V_{-} with a fixed voltage $V_{+} = \mathrm{VCC}\frac{R_3}{R_2+R_3}$, where R_3 is slightly lower than R_2. Therefore, when the laser is off, $\mathrm{I_{PD}} = 0$ and $V_{-} = \frac{\mathrm{VCC}}{2} > \mathrm{VCC}\frac{R_3}{R_2+R_3} = V_{+}$, and thus the output voltage of CMP is $\mathrm{V_O} = 0$; when the laser is on, $V_{-} = \frac{\mathrm{VCC}}{2} - \mathrm{R}_f * \mathrm{I_{PD}} < V_{+}$, and the output voltage is $\mathrm{V_O} = \mathrm{VCC}$. The demodulation is performed by an integrated microcontroller unit (MCU). Since the laser signal is modulated by a $\mathrm{T_X}$ port of a universal asynchronous receiver/transmitter (UART) device, the $\mathrm{R_X}$ port of the MCU can detect the digital signal $\mathrm{V_O}$ and save the corresponding data into the memory. Such a circuit design does not rely on expensive analog-to-digital convertors, and the computational burden for demodulation can be minimized.

Supplementary Note 6. Full-duplex cross-media video transmission process

The video of star twinkling is performed over the microwave-to-laser link from the air to underwater, and the lotus blooming video is performed over the laser-to-microwave link from the underwater to air. As seen in Supplementary Movie 1, when the laser source is turned off, the lotus blooming video becomes noise, but star twinkling remains displayed. When the power amplifier is turned off, the star twinkling video is held and there is no data transmission, but lotus blooming remains displayed. It is clear that these two different videos are transmitted and received independently and simultaneously cross the bidirectional air-water interface. In Case 1, the *x*-polarized horn antenna was fixed 0.1 m away from the metasurface sample, and in Case 2, the antenna distance was increased to about 0.3 m.

Supplementary Note 7. Potential applications of links and their rate limiting factors

Because signal modulation is realized based on the state changing of the used Schottky diode and photodiode, thus their switching frequency is the main factor that limits the modulation speed of the metasurface. The switching frequency of a diode mainly depends on its junction capacitance value, involving the accumulation and recombination time of charge carriers. Additionally, the large capacitance brought by the parallel arrangement of photodiodes on the metasurface will affect the speed Developing high-order modulation formats on metasurface can help improve link rates[6]. However, it will bring greater expenses, including power consumption and system complexity, due to requirement for precise modulation of more states on the metasurface.

In fact, 400 and 100kbps communication links are sufficient to transmit high-quality text, images, and audio. We also verified that they can be used for general-quality video transmission. Therefore, the microwave-optical bidirectional conversion links have potentials in air-water cross-media wireless communication. For example, underwater detection equipment (e.g., an unmanned undersea vehicle) can wirelessly transmit collected ocean data (e.g., underwater images) to a drone in real time. At the same time, the drone can also send real-time control commands to an underwater equipment to instruct it to implement specific tasks (e.g., underwater cruising). This is crucial for marine environment monitoring, underwater resource exploitation, and marine scientific research, as it helps to achieve true unmanned and full-time operations.

Supplementary Note 8. Extending metasurface to higher microwave frequencies

It is feasible to extend the system to higher microwave frequencies based on our approach. Because the metasurface-enabled microwave-optical signal conversions are achieved based on diode modulations, thus the cut-off frequency of the used diodes determines mainly the microwave working frequencies of the system. To increase the microwave operating frequency of the metasurface, we can choose to use the Schottky diode[7] and photodiode[8] with high cut-off frequencies. Based on these high cut-off frequency diodes, we have down-scaled and optimized the meta-element to achieve higher microwave frequencies, as shown in Supplementary Fig. 13a. The corresponding simulated results are shown in Supplementary Fig. 13b. It is clear that the meta-element can produce an obvious absorption resonance at 12.68 GHz for x-polarized incident microwave; for y-polarized microwave, the reflection amplitude difference of 20 dB can be achieved at 14.28 GHz. Therefore, the metasurface can operate at higher microwave frequencies for greater bandwidth. In simulations, the off and on states of the Schottky diode are derived from its datasheet SPICE model[9]; the tunable capacitance parameters of the photodiode are taken from Supplementary Ref. 8, and for the unilluminated and illuminated states, the capacitances of the photodiode are 12 and 35 fF, respectively.

Supplementary Note 9. Metasurface-enabled satellite communication and underwater long-distance wireless communication

As we drew in Fig. 1 in the main text, the bidirectional conversion metasurface offers an effective wireless platform to link the satellite and underwater equipment. We provide more discussion on this potential application scenario. The optical-to-microwave transmission is achieved based on the optically-controlled microwave amplitude modulation. That is to say, under different laser intensities, the reflected microwave amplitudes of the metasurface are different, and thus the '0' and '1' data can be sent by switching the back-reflected microwave powers. The microwave reflection ability of the metasurface can be characterized by its radar cross section (RCS). For amplitude-modulated microwave signal, the difference of the radar cross sections (RCSs) of the metasurface under two different reflection states is[10]:

$$\Delta\text{RSC} = \frac{\lambda^2}{4\pi} G_m^2 |\Gamma_1 - \Gamma_2|^2 \quad \text{(S5)}$$

where G_m is the gain of the metasurface; Γ_1 and Γ_2 are the microwave power reflection coefficients of the metasurface under two different laser illuminating states, respectively, which can be obtained from the meta-element simulation. The gain G_m of the metasurface depends on its effective aperture A_m, and their relationship is:

$$G_m = \frac{4\pi}{\lambda^2} A_m \quad \text{(S6)}$$

for planar metasurface at far field, the effective aperture A_m is equal to its actual physical area. Thus, by substituting Eq. (S6) into Eq. (S5), we obtain differential radar cross section ΔRSC:

$$\Delta\text{RSC} = \frac{4\pi}{\lambda^2} A_m^2 |\Gamma_1 - \Gamma_2|^2 \quad \text{(S7)}$$

it is clear that increasing the physical area and reflection coefficient difference of the metasurface helps to improve the ΔRSC, which is more conducive to signal demodulation.

For satellite communication based on the reflection amplitude modulation, the received signal power P_r by the satellite is directly related to the ΔRSC and can be expressed using classical radar equation[10]:

$$P_r = \frac{P_t G^2 \lambda^2}{(4\pi)^3 d^4} \Delta\mathrm{RSC} \tag{S8}$$

where P_t is the microwave power transmitted by the satellite, G is the gain of the satellite antenna, and d is the distance between satellite and metasurface. To demodulate and recover the transmitted data, the received signal power P_r must be greater than the sensitivity of the satellite receiver. From Eq. (S7) and Eq. (S8), we know that the received signal power is related to multiple factors, including distance, antenna gain, and metasurface area. As reported in Supplementary Ref. 11,12, the sensitivity of satellite receiver can be as low as -160 dBm, and antenna gain can reach 50 dBi. In this case, by combining Eq. (S7) and Eq. (S8), we can calculate the required transmitted microwave power for the metasurface-based satellite communication. When the satellite altitude is 2000 km and the metasurface effective area is 300 × 150 mm^2, the calculated minimum satellite transmitted microwave power is about 1.4 W. To reduce the transmitted power, we can increase the metasurface area by using more meta-elements.

For the optical-to-microwave conversion, the required illuminated laser power P_{laser} is 21.6 mW (13.3 dBm), as discussed in the main text. Due to the attenuation effect of water to light transmission, to achieve a longer underwater optical wireless communication distance, it is necessary to increase the laser power. As discussed in Supplementary Ref. 13, the attenuation rate of blue or green light is approximately 0.39 dB/m in clear ocean. Therefore, we can calculate the required laser power for different underwater communication distances. When the object is 10 m underwater, the required laser power is 52.5 mW (17.2 dBm), and when optical communication distance increases to 50 m, the required laser power is 1910 mW (32.8 dBm), which is comparable to the power levels required for current underwater wireless optical communications[13]. As the distance increases further to achieve extremely long-distance underwater optical communication, the required power will significantly increase. Recently, several solutions have been proposed to improve the underwater wireless optical communication distance, such as spatial diversity techniques and optical lenses. Specifically, it is feasible to use multiple photosensors and then combine their receiving signals to increase the sensitivity, and it is also feasible to use large lens over the photosensors to gather more optical power.

Supplementary References

1. Zhao, H., Shuang, Y., Wei, M., Cui, T. J., Hougne, P. D. & Li, L. Metasurface-assisted massive backscatter wireless communication with commodity Wi-Fi signals. *Nat. Commun.* **11**, 3926 (2020).
2. Sang, J. et al. Coverage enhancement by deploying RIS in 5G commercial mobile networks: field trials. *IEEE Wireless Commun.* **31**, 172-180 (2024).
3. Friis, H. T. A note on a simple transmission formula. *Proc. IRE* **34**, 254-256 (1946).
4. Zhang, X. G. et al. Optoelectronic metasurface for free-space optical-microwave interactions. *ACS Appl. Mater. Interfaces* **15**, 22744-22751 (2023).
5. Brown, W. C. Adapting microwave techniques to help solve future energy problems. *IEEE Trans. Microw. Theory Techn.* **21**, 753-763 (1973).
6. Chen, M. Z. et al. Accurate and broadband manipulations of harmonic amplitudes and phases to reach 256 QAM millimeter-wave wireless communications by time-domain digital coding metasurface. *Natl. Sci. Rev.* **19**, nwab134 (2022).
7. Wagih, M., Hilton, G. S., Weddell, A. S. & Beeby, S. Broadband millimeter-wave textile-based flexible rectenna for wearable energy harvesting. *IEEE Trans. Microw. Theory Techn.* **68**, 4960-4972 (2020).
8. Malyshev, S. A. & Chizh, A. L. P-I-N photodiodes for optical control of microwave circuits. *IEEE J. Sel. Topics Quantum Electron.* **10**, 679-685 (2004).
9. *Surface-Mount Schottky Diodes SMS7630 Series Datasheet* (SKYWORKS, 2021); https://www.skyworksinc.com/-/media/SkyWorks/Documents/Products/201-300/Surface_Mount_Schottky_Diodes_200041AG.pdf
10. Nikitin, P. V., Rao, K. V. S. & Martinez, R. D. Differential RCS of RFID tag. *Electron. Lett.* **43**, 431-432 (2007).
11. Kumari, A. & Bhatt, D. Advanced system analysis and survey on the GPS receiver front end. *IEEE Access* **10**, 24611-24626 (2022).
12. Rao, S. K. Advanced antenna technologies for satellite communications payloads. *IEEE Trans. Antennas Propag.* **63**, 1205-1217 (2015).
13. Kaushal, H. & Kaddoum, G. Underwater optical wireless communication. *IEEE Access* **4**, 1518-1547 (2016).